Left Ventricle: Automated Segmentation by Using Myocardial Effusion Threshold Reduction and Intravoxel Computation at MR Imaging[1]

Noel C. F. Codella, MEng
Jonathan W. Weinsaft, MD
Matthew D. Cham, MD
Matthew Janik, MD
Martin R. Prince, MD, PhD
Yi Wang, PhD

This retrospective analysis of existing patient data had institutional review board approval and was performed in compliance with HIPAA. No informed consent was required. The purpose of the study was to develop and validate an algorithm for automated segmentation of the left ventricular (LV) cavity that accounts for papillary and/or trabecular muscles and partial voxels in cine magnetic resonance (MR) images, an algorithm called LV Myocardial Effusion Threshold Reduction with Intravoxel Computation (LV-METRIC). The algorithm was validated in biologic phantoms, and its results were compared with those of manual tracing, as well as those of a commercial automated segmentation software (MASS [MR Analytical Software System]), in 38 subjects. LV-METRIC accuracy in vitro was 98.7%. Among the 38 subjects studied, LV-METRIC and MASS ejection fraction estimations were highly correlated with manual tracing ($R^2 = 0.97$ and $R^2 = 0.95$, respectively). Ventricular volume estimations were smaller with LV-METRIC and larger with MASS than those calculated by using manual tracing, though all results were well correlated ($R^2 = 0.99$). LV-METRIC volume measurements without partial voxel interpolation were statistically equivalent to manual tracing results ($P > .05$). LV-METRIC had reduced intraobserver and interobserver variability compared with other methods. MASS required additional manual intervention in 58% of cases, whereas LV-METRIC required no additional corrections. LV-METRIC reliably and reproducibly measured LV volumes.

Supplemental material: *http://radiology.rsnajnls.org/cgi/content/full/248/3/1004/DC1*

[1] From the Department of Physiology, Biophysics, and Systems Biology (N.C.F.C., Y.W.), Department of Radiology (J.W.W., M.D.C., M.J., M.R.P., Y.W.), and Cardiology Division, Department of Medicine (J.W.W., M.J.), Weill Medical College of Cornell University, 575 Lexington Ave, 3rd Floor, New York, NY. Received November 18, 2007; revision requested January 4, 2008; revision received January 9; accepted February 20; final version accepted March 3. **Address correspondence to** Y.W. (e-mail: *yiwang@med.cornell.edu*).

Accurate quantification of left ventricular (LV) ejection fraction and chamber volumes is important for therapeutic management and prognostic assessment of heart disease (1,2). Cardiac magnetic resonance (MR) imaging enables highly accurate and reproducible LV quantification (3) and has been used as a diagnostic standard method for volumetric assessment (4). Manual tracing of LV endocardial contours is commonly used to assess LV cavity volumes from cine MR images. However, manual tracing can be time consuming (5) and is susceptible to the inherent subjectivity of manually determined border delineation. Manual tracing can be especially compromised when accounting for irregularly contoured LV structures such as papillary and/or trabecular muscles, which have been shown to decrease reproducibility (6) and increase time for LV quantification by nearly twofold (5). Automated segmentation methods hold potential utility for objectively quantifying the LV cavity in a manner that rapidly accounts for contour irregularities. However, although previous automatic methods have employed clustering (7), deformable models (8–11), fuzzy pixel affinities (12,13), and dynamic programming (13–15), these methods do not consider partial voxel contributions to LV volume and cannot segment fine trabeculations.

The purpose of this study was to develop and validate an algorithm for automated segmentation of the LV cavity, termed LV Myocardial Effusion Threshold Reduction with Intravoxel Computation (LV-METRIC), that accounts for papillary and/or trabecular muscles and partial voxels (16) in cine MR images.

Advance in Knowledge

- Automated segmentations of the left ventricular (LV) cavity that account for partial voxels can be achieved with an algorithm that computes the location of the LV cavity, then determines the mean and standard deviation of blood and myocardial signal intensities.

Materials and Methods

Subject Selection

This retrospective analysis of existing patient data was approved by our institutional review board and was performed in compliance with the Health Insurance Portability and Accountability Act. No informed consent was required.

Data were acquired from MR imaging examinations previously performed in 38 subjects, including 18 subjects without clinically evidenced coronary artery disease and with normal LV systolic function (on the basis of a priori manual tracing), as well as 20 randomly selected patients who had been referred for clinical cardiac MR imaging. In all subjects, demographic characteristics were assessed with a uniform patient questionnaire completed at the time of MR imaging and were verified by review of patient records. The most common clinical indications for referral were assessment of the presence or pattern of myocardial scar. Characteristics of the overall study population, with stratification according to subject subgroup, are provided in Table 1.

LV-METRIC Algorithm

The LV-METRIC segmentation algorithm is performed in six steps:

1. Estimation of the initial LV center point: A Hough transform is performed on the subtraction magnitude of images from phases one and 10 of an initial midventricular section, selected by the user, to identify a point within full-blood voxels of the LV cavity (9,13,14,17).

2. Measurement of mean and standard deviation of blood signal intensity: Edge-based region growth (eight-connected two-dimensional [2D], 10-connected three-dimensional [3D]) is performed from the initial seed point to calculate the mean and standard deviation (μ_b and σ_b) of the signal intensity of voxels with nearly full blood content (Fig 1).

3. Compensation for coil sensitivity: A least-squares planar surface is fit to the signal intensities of full-blood voxels to compensate for coil sensitivity variations across the area of the LV.

4. Estimation of myocardial signal intensity: To estimate the mean myocardial signal intensity, μ_m, successive lower-bound threshold-based region-growth processes are run for an iteratively decreasing threshold, by using the same seed used in the second step. Eventually, region growth breaks through the myocardium, "effusing" into bright surrounding structures (fat, right ventricle, muscle) and causing a sudden increase in the apparent blood volume, which can be characterized by a discontinuity in a ratio of consecutive volume growth, $\delta(i)$, as follows:

$$\delta(i) = \frac{V(i + 0.1) - V(i)}{V(i) - V(i - 0.1)}, \qquad (1)$$

where $i = \mu_b$/threshold starts at 1.0 and increments by 0.1 each iteration and V

Implication for Patient Care

- Ventricular volumes across all phases of short-axis sections can be automatically measured reliably and reproducibly.

Published online
10.1148/radiol.2482072016

Radiology 2008; 248:1004–1012

Abbreviations:
LV = left ventricle
LV-METRIC = LV Myocardial Effusion Threshold Reduction with Intravoxel Computation
SSFP = steady-state free precession
3D = three-dimensional
2D = two-dimensional

Author contributions:
Guarantor of integrity of entire study, Y.W.; study concepts/study design or data acquisition or data analysis/interpretation, all authors; manuscript drafting or manuscript revision for important intellectual content, all authors; manuscript final version approval, all authors; literature research, N.C.F.C., J.W.W., M.D.C., Y.W.; clinical studies, J.W.W., M.D.C., M.J., M.R.P.; experimental studies, N.C.F.C., J.W.W., M.D.C., M.R.P., Y.W.; statistical analysis, N.C.F.C., J.W.W., M.J., Y.W.; and manuscript editing, N.C.F.C., J.W.W., M.D.C., M.R.P., Y.W.

Authors stated no financial relationship to disclose.

is volume. The discontinuity of volume growth during increasing i is used to measure the threshold at which region growth has penetrated the myocardium (Fig 1).

The threshold at which region growth effuses into surrounding structures is strongly correlated with the mean and standard deviation of the signal intensity of the myocardium and the thickness of the myocardium, as seen in simulations (Fig 2). A fixed constant can be used to predict the distance (in units of standard deviations) between the effusion threshold and the true mean for a range of expected myocardial wall thicknesses, with little error in aggregate volume measurement from myocardial mean estimate error (Appendix E1, *http://radiology.rsnajnls.org/cgi/content/full/248/3/1004/DC1*). For this study, $0.9\sigma_b$ was used. In cases of abnormally thin myocardium, the value was automatically adjusted to a higher value to compensate. These situations are detectable, as cine SSFP imaging typically produces a blood-to-myocardium contrast ratio of at least 2.0.

5. Completion of segmentation and measurement of blood volume: The total blood volume of the segmented image section of the LV is then determined with the summation

$$V = \sum_x h(x)w(x), \qquad (2)$$

where V is volume, $h(x)$ is the histogram of the LV, and $w(x)$ is the weight (voxel percentage blood content) associated with voxels of signal intensity x. Assuming a noiseless system and a good point spread function,

$$w(x) = \frac{x - M}{B - M}, \qquad (3)$$

where B and M are the signal intensities associated with full-blood and full-myocardium voxels, respectively. Accounting for Gaussian noise, B and M are assigned—$(\mu_b - n\sigma_b)$ and $(\mu_m + n\sigma_b)$, respectively—with $n = 2$. The assignments ensure that at least 99.4% of full-blood and full-myocardium voxels will be weighted correctly, while maintaining the proportionality of partial voxel interpolation.

Region growth is then performed again for the last time within that section or phase, by using an absolute threshold of $(\mu_m + n\sigma)$. The blood content of each voxel visited is interpolated by using Equation (3), except for voxels visited during the second step, which are always counted as full-blood voxels.

6. Propagation of seed points across

Table 1

Subject Characteristics

Parameter	Overall ($n = 38$)	Randomly Selected Patients ($n = 20$)	Healthy Subjects ($n = 18$)	*P* Value*
Age (y)†	52.4 ± 15.1	56.5 ± 14.6	47.8 ± 14.6	.08
Coronary artery disease	26 (10)	50 (10)	. . .	<.001
Male sex	39 (15)	50 (10)	28 (5)	.16
Hypertension	29 (11)	40 (8)	17 (3)	.16
Hyperlipidemia	26 (10)	35 (7)	17 (3)	.28
Diabetes mellitus	5 (2)	10 (2)	. . .	.49
Tobacco use	5 (2)	5 (1)	6 (1)	>.99
Family history of coronary artery disease	26 (10)	35 (7)	17 (3)	.28

Note.—Unless otherwise specified, data are percentages, with numbers of subjects in parentheses.

* Calculated with the Student *t* test.

† Data are means ± standard deviations.

Figure 1

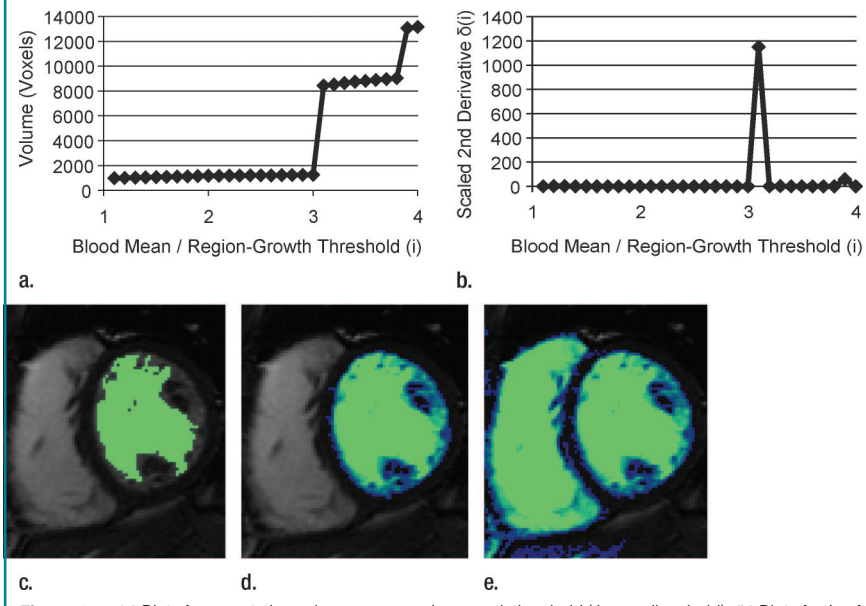

Figure 1: **(a)** Plot of segmentation volume versus region growth threshold ($i = \mu_b$/threshold). **(b)** Plot of ratio of consecutive volume growth $\delta(i)$ versus step index i (see Eq [1]). As i begins to increase, $\delta(i)$ is relatively constant and close to 1, until effusion through the wall occurs. **(c–e)** Two-dimensional cine steady-state free precession (SSFP) short-axis MR images show LV-METRIC second step, with segmentation corresponding to mean divided by threshold at **(d)** 3.0 and **(e)** 3.1 arbitrary units. Once region growth escapes the LV, discontinuity in growth rate is observed because of region growth effusion into tissues and fluids surrounding the LV wall. Partial voxels are displayed from blue to green as containing least to most blood, respectively.

sections and phases: The seed point for the next section or phase is determined by examining an 11 × 11-pixel window in the next image centered around the previous section segmentation's center of mass. An energy function based on distance from the center of the window and the signal intensity difference from the previous section's blood mean is applied to each pixel in the window (Appendix E1, *http://radiology.rsnajnls.org/cgi/content/full/248/3/1004/DC1*). The pixel with minimum energy is chosen as the next seed point. Steps 2–6 are then repeated on the new image by using the selected seed point. The process is continued for all desired sections and phases in a given cine study.

Phantom Experiments

So that we could estimate the absolute accuracy of segmentations, phantoms were constructed by using meat and fat. A plastic container with a diameter of 28 cm was filled with vegetable shortening (fat), and two depressions were molded in the shortening. The first phantom was built by filling one of the depressions (approximately 10 cm in diameter) with ground beef that had been further ground to a paste consistency with a food processor and then inserting a thin-walled plastic container (subvoxel thickness) into the beef (which was approximately 6 cm in diameter). The plastic container was used to prevent water absorption into the beef. The second phantom was built by inserting a pork chop into the second shortening depression (approximately 9.3 × 9.5 cm), cutting a slit across the surface of the chop, and prying the slit open to form a cavity (approximately 4 × 3 cm). The cavity was lined with a thin layer of shortening to minimize water absorption by the pork. Water (100 mL) was poured into the cup in the beef phantom and into the cavity of the pork chop phantom (20 mL).

Figure 2

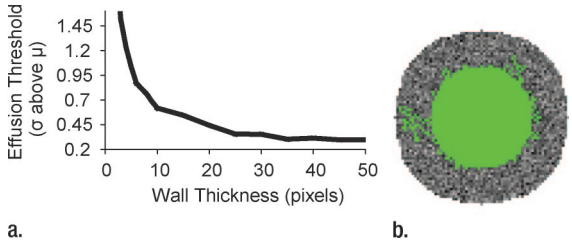

Figure 2: Simulation results of threshold-based region growth seeded at the center of a ring of normally distributed signal intensities. **(a)** In this graph, x-axis corresponds to wall thickness, and y-axis corresponds to the threshold at which region growth effuses through the ring, in terms of standard deviations above the mean ring signal intensity. Values converge to 0.2 at infinity. **(b)** Simulated image demonstrates region growth at effusion threshold, seeded at center of a ring with normally distributed pixel intensities and a wall thickness of 15 pixels.

Table 2

Phantom Measurement Results

Section Mode/Section Thickness (mm)/ Intersection Gap (mm)	Beef Phantom with 100 mL of Water			Pork Chop Phantom with 20 mL of Water		
	Manual Tracing	MASS	LV-METRIC	Manual Tracing	MASS	LV-METRIC
2D/8.0/2.0	119.2	126.32	98.3	30.6	30.76	22
2D/6.0/4.0	113.6	112.08	97.2	26.2	30.16	22.2
3D/2.0/0.0	102.5	94.49	98.7	22.6	23.2	20.1

Note.—All data are in milliliters.

The phantoms were imaged with 2D and 3D SSFP by using a 1.5-T MR imaging unit (Signa; GE Healthcare, Milwaukee, Wis) with an eight-channel cardiac phased-array coil. Imaging parameters were as follows: repetition time msec/echo time msec, 3.9–4.5/1.6–1.9; flip angle, 55°–60°; matrix size, 256 × 128; image dimensions, 256 × 256; receiver bandwidth, 125 kHz; and field of view, 290 mm. Three-dimensional images were acquired at section thicknesses of 2.0 and 4.0 mm, and 2D images were acquired at clinical section thicknesses and spacing, respectively, of 8.0 and 2.0 mm or 6.0 and 4.0 mm.

Patient Experiments

Patients were imaged with 2D cine SSFP by using the same MR imaging unit used to image the phantoms. Imaging parameters were as follows: 3.3–4.5/1.1–2.0; flip angle, 55°–60°; matrix size, 192 × 192–256 × 256; image dimensions, 256 × 256; receiver bandwidth, 125 kHz; field of view, 290–400 × 240–360 mm; and section thickness and section gap, 6–8 and 2–4 mm, respectively (total, 10 mm). The LV in each patient was imaged in six to 10 sections and 20–28 cardiac phases.

Image Analysis

Quantitative measurements were performed by experienced (≥2 years) physicians (J.W.W. and M.D.C.) who had completed dedicated fellowship training in cardiac MR imaging and who had performed quantification for at least 1000 cardiac MR imaging studies prior to participation in this study protocol.

Automated and manual segmentations were performed at a workstation (Advantage; GE Healthcare) with an Intel Xeon 3.4-GHz processor and 4 GB of random access memory. Processing and execution time were assessed with a standard timer.

For phantom data, water volume was quantified with manual tracing, a software system distributed on the GE Advantage workstation (MASS [MR Analytical Software System], version 6.1; Medis Medical Imaging Systems, Leiden, the Netherlands), and LV-METRIC segmentation. Results were compared

Table 3

Segmentation Results in 38 Subjects for All Methods

Parameter	LV-METRIC with Partial Voxel Interpolation	LV-METRIC without Partial Voxel Interpolation	MASS	Manual Tracing
Diastolic volume (mL)	121.8 ± 42.9	144.2 ± 47.9	164.9 ± 57.6	144.9 ± 49.9
Systolic volume (mL)	48.9 ± 38.8	62.4 ± 46.1	73.6 ± 53.4	60.5 ± 44.7
Ejection fraction (%)	63.5 ± 14.9	60.1 ± 14.8	59 ± 14.8	61.6 ± 14.3
Percentage of cases requiring manual intervention*	0	0	58†	100

Note.—Unless otherwise specified, data are means ± standard deviations across all subjects in each group.

* One or more sections required manual intervention, aside from manual valve plane definitions.

† Segmentations in 22 of 38 subjects resulted in at least one section segmentation failure (mean number of sections with failed segmentation, 2.1; range, one to eight).

with ground truth (volume of water poured into each phantom). All readers were blinded to ground truth during quantification.

For patients, LV-METRIC measurements were compared with manual tracings, which served as the reference standard, as established in prior studies (7–9,12,13). In addition, the commercially available automatic LV segmentation software package MASS (15) was also employed, so that we could compare LV-METRIC with another commercially available product. The readers performed all segmentations while blinded to the results of other methods.

Manual tracing was performed with papillary and/or trabecular muscles excluded from the blood volume. Trabeculae were defined as portions of myocardium that protruded more than 1.5 mm from the circumferential contour of the LV cavity and had equivalent signal intensity to the adjacent LV wall (6,18). Basal image positions were defined by the most basal image that encompassed at least 50% of circumferential myocardium (6) and did not vary in automated analyses.

User input for both LV-METRIC and MASS consisted of section range specification for segmentation (required), and manual definition of the aortic annulus and mitral annulus on basal sections for which the section plane did not contain the full circumference of the myocardium. Available optional input for MASS consisted of manual tracing, and available optional input for LV-METRIC consisted of endocardial border definition, seed point placement, and window adjustment for partial voxel interpolation. Optional input for both MASS and LV-METRIC was used only when an automated segmentation was judged by an experienced clinician to have failed (approximate error in endocardial definition, >10%). All user input was recorded.

Volume measurements from each automated method were taken at fixed manually selected end-diastolic and end-systolic phases and compared with manual tracing measurements. To determine how partial voxels contributed to the volume estimation differences between LV-METRIC and manual tracing, additional LV-METRIC measurements were repeated in a manner that consid-

Figure 3

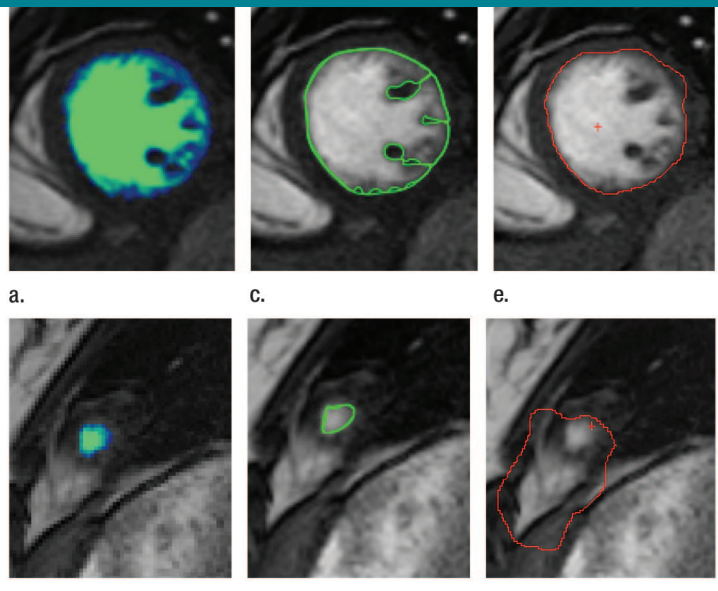

Figure 3: Two example segmentation results with 2D cine SSFP short-axis MR imaging at **(a, c, e)** midventricular and **(b, d, f)** apical levels show details of **(a, b)** LV-METRIC, **(c, d)** MASS, and **(e, f)** manual tracing methods. By visual inspection, manual tracing and MASS overestimate volume, as a multitude of papillary and/or trabecular muscles and partial voxels are not accurately traced. In comparison, LV-METRIC accounts for the structure. Partial voxels are displayed from blue to green as containing least to most blood, respectively. **(d)** Example in which the MASS algorithm failed, requiring manual intervention.

ered voxels with any blood content as full-blood voxels. To assess the influence of LV-METRIC automated phase selection on measurements, LV-METRIC measurements were acquired by using automatically selected phases and were then compared with the LV-METRIC results acquired by using manual phase selections.

For the assessment of the intraobserver and interobserver variability of each method, the first reader (J.W.W.) repeated measurements in a subset of 10 patients after 2 weeks, and a second reader (M. D. C.) independently repeated measurements in the same subset of 10 patients. All readers were blinded to prior measurements.

For validation of the LV-METRIC estimations of blood and myocardial signal statistics, manual regions of interest were drawn over full-blood and full-myocardial voxels to measure the respective values on a randomly selected sample of 36 images in patients (septal wall thickness range, 4–14 pixels; mean, 8.94 pixels ± 2.6 [standard deviation]), and the results were compared with the respective LV-METRIC estimations. All regions of interest were drawn by operators who were blinded to LV-METRIC results.

Statistical Analysis

Comparisons between measurements in this study were performed by calculating the mean and standard deviation of paired differences among measurements compared. The Student *t* test was used to assess statistical significance ($P < .05$). Linear regression was performed to assess correlations, and Bland-Altman analysis was used to compare volume estimations between manual tracing and the other automated methods.

Results

Phantom Experiments

Results from phantom experiments are summarized in Table 2. In comparison to manual tracing and MASS, LV-METRIC more accurately measured the known phantom cavity water volumes. The greatest errors for manual tracing and MASS, which were higher than 50% (>10-mL error divided by 20-mL total volume), came from clinical-resolution images at 6- and 8-mm section thicknesses of the 20-mL pork chop phantom, which had the most irregular shape and the smallest volume. In comparison, LV-METRIC had a maximum error of 11% (2.2 mL divided by 20 mL) for small cavities and 2.8% (2.8 mL divided by 100 mL) for larger cavities that decreased to 0.5% (0.1 mL divided by 20 mL) and 1.3% (1.3 mL divided by 100 mL) for 3D high-spatial-resolution (section thickness, 2 mm) images.

Patient Experiments

Measurements from LV-METRIC, MASS, and manual tracing are summarized in Table 3, and example segmentations are shown in Figure 3. Manual border definitions of the aortic annulus and mitral annulus on basal sections were required for, on average, one basal section per patient for both LV-METRIC and MASS. All LV-METRIC segmentations were successful, with no further manual intervention. MASS segmentation failed (approximate error in endocardial definition, >10%) in 22 (58%) of 38 cases, requiring manual corrections in one to eight sections (mean, 2.1 sections). Figure 3d shows a typical failure of the MASS algorithm.

As shown in Table 4 and Figure 4, mean end-diastolic and end-systolic volumes in LV-METRIC measurements were, respectively, 23.1 mL and 11.6 mL smaller than manual tracing measurements ($P < .001$). The resulting ejection fraction was 1.9 percentage points larger ($P < .001$). LV-METRIC volume measurements that considered partial voxels as full voxels were not significantly different from manual tracing results, with diastolic volume smaller by 0.77 mL ± 5.1 ($P = .35$) and systolic volume larger by 1.9 mL ± 6.1 ($P = .06$). Volume and ejection fraction correlation between LV-METRIC and

Table 4

Results of Comparison of Automated Measurements with Manual Tracing Measurements

Automated Method	Difference in End-Diastolic Volume between Manual Tracing and Automated Measurements		Difference in End-Systolic Volume between Manual Tracing and Automated Measurements		Difference in Ejection Fraction between Manual Tracing and Automated Measurements		Linear Regression Correlation*	
	Absolute (mL)	Relative (%)	Absolute (mL)	Relative (%)	Absolute (%)	Relative (%)	Volume	Ejection Fraction
LV-METRIC with partial voxel interpolation†	23.1 ± 10.2	16 ± 4.8	11.6 ± 7.2	20.7 ± 7.2	−1.9 ± 2.5	−3.0 ± 4.2	$y = 0.86x - 2.94$, $R^2 = 0.990$	$y = 1.02x + 0.39$, $R^2 = 0.972$
LV-METRIC without partial voxel interpolation‡	0.8 ± 5.1	0 ± 3.4	−1.9 ± 6.1	−4.4 ± 9.5	1.5 ± 3.3	3 ± 7.5	$y = 0.978x - 2.9$, $R^2 = 0.992$	$y = 1.01x - 1.9$, $R^2 = 0.95$
MASS†	−19.9 ± 10.5	−13.7 ± 5.1	−13.1 ± 10.7	21.6 ± 12.6	2.6 ± 3.2	4.5 ± 5.3	$y = 1.13x - 3.5$, $R^2 = 0.989$	$y = 1.01x - 3.2$, $R^2 = 0.95$

Note.—All subtraction values are means ± standard deviations of paired differences (manual tracing measurement minus each automated method measurement).

* Where *x* is manual tracing and *y* is LV-METRIC.

† All differences were significant ($P < .05$, Student *t* test).

‡ No differences (except ejection fraction) were significant ($P > .05$, Student *t* test).

Figure 4

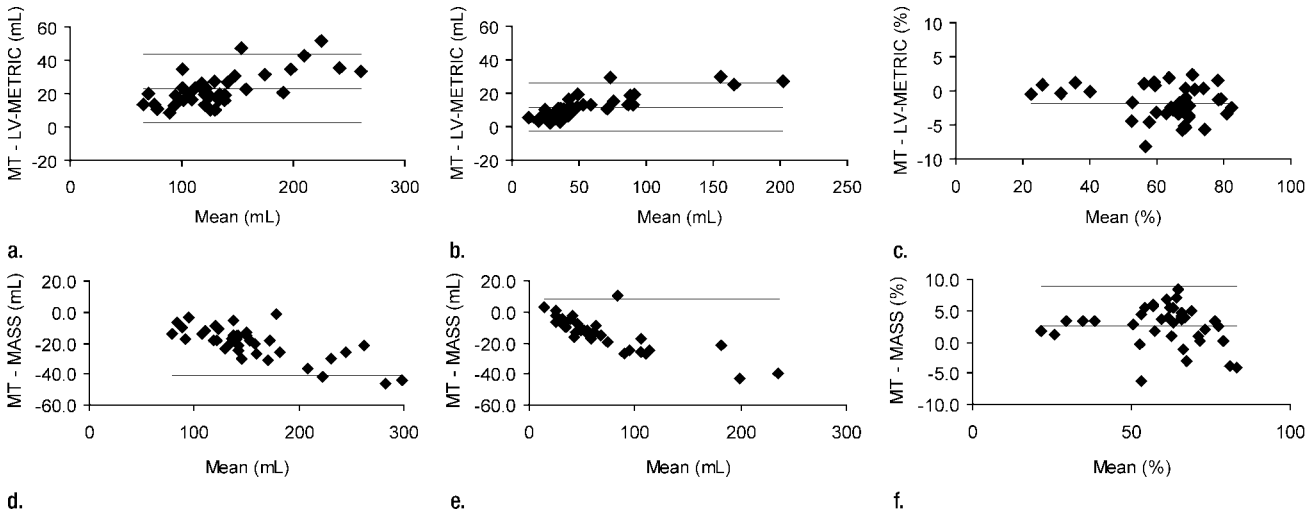

Figure 4: Bland-Altman plots for all 38 subjects show results of comparison of **(a–c)** manual tracing *(MT)* and LV-METRIC and **(d–f)** manual tracing and MASS. Plots show comparisons of **(a, d)** diastolic volume, **(b, e)** systolic volume, and **(c, f)** ejection fraction between manual tracing and each automated algorithm. Manual volume measurements were consistently overestimated as compared with LV-METRIC measurements. Ejection fraction was underestimated as compared with LV-METRIC, on average.

Table 5

Reproducibility Measurements

Parameter	Intraobserver Variability			Interobserver Variability		
	Manual Tracing	LV-METRIC	MASS	Manual Tracing	LV-METRIC	MASS
Diastolic volume (mL)	1.8 ± 2.4*	0.021 ± 0.17	0.02 ± 0.35	−1.4 ± 2*	0.26 ± 0.44	0.561 ± 0.7*
Systolic volume (mL)	1.5 ± 2*	0.032 ± 0.26	0.133 ± 0.77	−1.4 ± 1.9*	0.086 ± 0.41	0.687 ± 0.73*
Ejection fraction (%)	0.63 ± 1.2	0.01 ± 0.24	−0.161 ± 0.51	0.62 ± 1.4	−0.037 ± 0.4	−0.401 ± 0.59

Note.—Data are means ± standard deviations of paired differences between observer measurements.

* $P < .05$, Student t test.

manual tracing was high ($R^2 = 0.99$ and $R^2 = 0.97$, respectively).

MASS measurements of end-diastolic and end-systolic volumes were, respectively, 19.9 mL and 13.7 mL larger than manual tracing measurements ($P < .001$). Ejection fraction was 2.6% smaller ($P < .001$).

Variability in LV-METRIC was reduced compared with both manual tracing and MASS (Table 5). MASS variability was decreased as compared with manual tracing but higher as compared with LV-METRIC because of the increased amount of user input required.

Correlation between LV-METRIC–selected and manually selected end-diastolic and end-systolic phases was high ($R^2 = 0.99$), with a slope near unity (0.98) and an intercept near zero (0.05). LV-METRIC measured diastolic volume was larger, on average, by 0.13 mL ± 2.79 ($P = .77$), and systolic volume was smaller by 0.47 mL ± 1.37 ($P < .05$), when using automatically selected phases as compared with using manually selected phases. The resultant ejection fraction was larger by 0.4% ± 1.39 ($P = .09$).

Comparison of LV-METRIC–estimated full-myocardial and full-blood signal intensity means with manual region of interest–measured counterparts showed high correlation between the two measurements (myocardium, $R^2 = 0.94$; blood, $R^2 = 1.0$; Fig 5), with a slope near unity (myocardium, 0.95; blood, 0.98, by using an intercept of 0). Blood signal intensity estimates differed by 1.2% ± 2.4 ($P = .02$). Myocardial signal intensity estimates differed by 2.1% ± 11.7 ($P = .09$).

A typical complete segmentation using LV-METRIC took on the order of 30–60 seconds, depending on the degree of user interaction. Actual segmentation processing time for selected section ranges and all phases was less than 15 seconds. A typical MASS segmentation took on the order of 2–3 minutes. The additional time was due primarily to increased necessary user interaction. Typical time for manual tracing was on

the order of 4–10 minutes (for only two cardiac phases).

Discussion

An automated segmentation algorithm (LV-METRIC) that considers the effects of partial voxels and papillary and/or trabecular structures on LV volume calculations has been presented. As compared with manual tracing and the commercially available segmentation software MASS, the partial voxel calculation of LV-METRIC demonstrated superior accuracy in phantoms where cavity volumes were known. In human subjects, LV-METRIC provided more detailed segmentations and drastically reduced the amount of manual interaction necessary as compared with manual tracing and MASS. When considering partial voxels as full voxels, LV-METRIC volume measurements were not significantly different from manual tracing measurements, suggesting that intravoxel interpolation accounted for the volume estimate difference between the two methods.

LV-METRIC does not depend on any shape assumptions, except that blood is enclosed by myocardium, making the algorithm robust over various morphologies and diseases (such as thin-walled myocardium or pericardial diseases). By simple region growth during successive blood threshold reduction, the apparent blood effuses through the myocardium into surrounding structures (eg, right ventricle, fat, pulmonary vessels), which causes an abrupt increase in the relative rate of change in the apparent blood volume. This abrupt increase in relative growth rate ranges from approximately 10^3 for effusion into the right ventricle to about 10^1 for smaller structures such as epicardial fluid or fat. Because the rate before effusion is about 1, the increase can be robustly detected to allow automated estimation of endocardial surface area and myocardial signal intensity for use in partial voxel interpolated computation of ventricular blood.

Prior automated methods may require input of manual tracings (12), require manual corrections after automated analysis (15), not segment papillary and/or trabecular muscle (12,13), or fail in up to 15% of cases (9). In our study, the commercial MASS algorithm yielded coarse contours that did not segment papillary and/or trabecular muscles or partial voxels, leading to overestimation of ventricular blood as compared with manual tracing and LV-METRIC. In addition, the MASS algorithm failed in up to eight sections in over half the cases. Most prior techniques are based on elegant geometric models that use LV shape assumptions, which may fail to accurately describe the LV shape when complicated by papillary and/or trabecular muscles, changes during the cardiac cycle, and variations from patient to patient. Furthermore, prior techniques have not considered the effects of partial voxels; instead, these studies have focused on generating contours (or meshes) and calculating corresponding surface area (or volume). To our knowledge, this study presents the first automated segmentation of the LV by using partial voxel interpolation.

Although LV-METRIC–estimated volumes were smaller than manual tracing estimates, the differences became statistically nonsignificant when LV-METRIC considered partial voxels as full voxels. In current breath-hold 2D acquisitions of cine SSFP images, the voxel size is limited to $1.4 \times 1.4 \times 10\ mm^3$. Consequentially, voxels with mixed myocardium and blood are invariably present, which can lead to volume overestimation when the partial voxel effects are not considered. It should be noted that volume overestimation does not necessarily translate into ejection fraction estimation error. Clinicians' tracing at both end diastole and end systole can be fairly consistent, resulting in a reasonably accurate ejection fraction ratio. However, as established in our phantom experiments, partial voxel computation may be required for accurate LV volume estimation. Three-

Figure 5

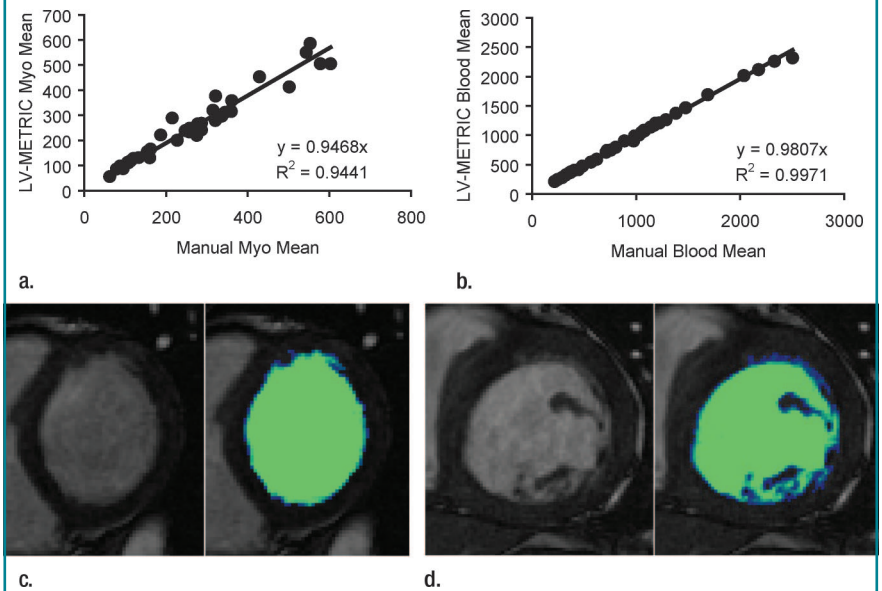

Figure 5: **(a, b)** Graphs of results with 36 sections in patients show manually measured **(a)** full-myocardial and **(b)** full-blood voxel signal intensity means plotted against the LV-METRIC estimates (septal wall thickness range, 4–14 pixels; mean, 8.94 pixels ± 2.6). **(c, d)** Original 2D cine SSFP short-axis MR images with LV-METRIC segmentations resulting from the worst myocardial mean estimates from each patient group. Excellent segmentation results were still observed. Partial voxels are displayed from blue to green as containing least to most blood, respectively.

dimensional high-spatial-resolution imaging may also reduce partial voxel error, but would require substantially more processing time if manual tracing were used.

The LV-METRIC algorithm has demonstrated robust performance. However, partial voxel linear interpolation may be susceptible to errors from myocardial mean estimation in cases of low contrast, errors caused by the phase difference between blood and myocardial spins, radiofrequency profile imperfections, and flow artifacts. Additional errors may occur from ghosting due to improper breath holding and irregular heartbeats. Further investigation with additional comparison standards, such as phase-contrast velocity imaging or thermodilution, in a larger group of patients, is warranted to assess the influence of such errors.

LV-METRIC may be applicable to other modalities of imaging the LV. However, the presented LV-METRIC method needs to be improved with automated valve tracing and epicardial segmentations. Currently, basal sections may require manual drawing of the valve annulus, which constitutes the only source of variability. Additionally, automated epicardial segmentation is necessary for LV mass estimation.

In summary, an automated algorithm for segmentation of the LV with partial voxel interpolation has been presented that reliably, reproducibly, and efficiently quantifies LV blood volume. Further validation with high-spatial-resolution imaging should be performed to confirm the existence and influence of partial voxels in volume calculation.

References

1. Moss AJ, Zareba W, Hall WJ, et al. Prophylactic implantation of a defibrillator in patients with myocardial infarction and reduced ejection fraction. N Engl J Med 2002; 346(12):877–883.
2. Solomon SD, Anavekar N, Skali H, et al. Influence of ejection fraction on cardiovascular outcomes in a broad spectrum of heart failure patients. Circulation 2005;112(24): 3738–3744.
3. Grothues F, Smith GC, Moon JC, et al. Comparison of interstudy reproducibility of cardiovascular magnetic resonance with two-dimensional echocardiography in normal subjects and in patients with heart failure or left ventricular hypertrophy. Am J Cardiol 2002;90(1):29–34.
4. Dewey M, Muller M, Eddicks S, et al. Evaluation of global and regional left ventricular function with 16-slice computed tomography, biplane cineventriculography, and two-dimensional transthoracic echocardiography: comparison with magnetic resonance imaging. J Am Coll Cardiol 2006;48(10):2034–2044.
5. Sievers B, Kirchberg S, Bakan A, Franken U, Trappe HJ. Impact of papillary muscles in ventricular volume and ejection fraction assessment by cardiovascular magnetic resonance. J Cardiovasc Magn Reson 2004;6(1): 9–16.
6. Papavassiliu T, Kuhl HP, Schroder M, et al. Effect of endocardial trabeculae on left ventricular measurements and measurement reproducibility at cardiovascular MR imaging. Radiology 2005;236(1):57–64.
7. Lynch M, Ghita O, Whelan PF. Automatic segmentation of the left ventricle cavity and myocardium in MRI data. Comput Biol Med 2006;36(4):389–407.
8. Kaus MR, von Berg J, Weese J, Niessen W, Pekar V. Automated segmentation of the left ventricle in cardiac MRI. Med Image Anal 2004;8(3):245–254.
9. van der Geest RJ, Lelieveldt BP, Angelie E, et al. Evaluation of a new method for automated detection of left ventricular boundaries in time series of magnetic resonance images using an Active Appearance Motion Model. J Cardiovasc Magn Reson 2004;6(3): 609–617.
10. Lynch M, Ghita O, Whelan PF. Left-ventricle myocardium segmentation using a coupled level-set with a priori knowledge. Comput Med Imaging Graph 2006;30(4):255–262.
11. Chen Q, Zhou ZM, Tang M, Heng PA, Xia DS. Shape statistics variational approach for the outer contour segmentation of left ventricle MR images. IEEE Trans Inf Technol Biomed 2006;10(3):588–597.
12. van Geuns RJ, Baks T, Gronenschild EH, et al. Automatic quantitative left ventricular analysis of cine MR images by using three-dimensional information for contour detection. Radiology 2006;240(1):215–221.
13. Pednekar A, Kurkure U, Muthupillai R, Flamm S, Kakadiaris IA. Automated left ventricular segmentation in cardiac MRI. IEEE Trans Biomed Eng 2006;53(7):1425–1428.
14. van der Geest RJ, Buller VG, Jansen E, et al. Comparison between manual and semiautomated analysis of left ventricular volume parameters from short-axis MR images. J Comput Assist Tomogr 1997;21(5):756–765.
15. van der Geest RJ, Jansen E, Buller VG, Reiber JH. Automated detection of left ventricular epi- and endocardial contours in short-axis MR images. IEEE Trans Comput Cardiol 1994;:33–36.
16. Pham DL, Xu C, Prince JL. Current methods in medical image segmentation. Annu Rev Biomed Eng 2000;2:315–337.
17. Illingworth J, Kittler J. A survey of the Hough transform. Comput Vis Graph 1988; 44(1):87–116.
18. Hudsmith LE, Petersen SE, Francis JM, Robson MD, Neubauer S. Normal human left and right ventricular and left atrial dimensions using steady state free precession magnetic resonance imaging. J Cardiovasc Magn Reson 2005;7(5):775–782.